JBC Papers in Press. Published on December 17, 2015 as Manuscript M115.676817
The latest version is at http://www.jbc.org/cgi/doi/10.1074/jbc.M115.676817

Pro-inflammatory macrophages sustain pyruvate oxidation through pyruvate dehydrogenase for the synthesis of itaconate and to enable cytokine expression

Johannes Meiser, Lisa Krämer, Sean C Sapcariu, Nadia Battello, Jenny Ghelfi, Aymeric Fouquier D'Herouel, Alexander Skupin, Karsten Hiller

University of Luxembourg, Luxembourg Centre for Systems Biomedicine, 6, avenue de Swing, L-4367 Belvaux, Luxembourg

Running title: *Pro-inflammatory macrophages sustain pyruvate oxidation*

To whom correspondence should be addressed: Karsten Hiller, Metabolomics Group, University of Luxembourg, Luxembourg Centre for Systems Biomedicine, 6, avenue de Swing, L-4367 Belvaux, Luxembourg, Tel: +352 46 66 44 6136, Email: karsten.hiller@uni.lu

Keywords: immunology; inflammation; macrophage; metabolic regulation; metabolism; mitochondrial metabolism; pyruvate; pyruvate dehydrogenase complex (PDC); pyruvate dehydrogenase kinase (PDC kinase); itaconate

ABSTRACT

Upon stimulation with Th1 cytokines or bacterial lipopolysaccharides, resting macrophages shift their phenotype towards a pro-inflammatory state as part of the innate immune response. LPS activated macrophages undergo profound metabolic changes to adapt to these new physiological requirements. One key step to mediate this metabolic adaptation is the stabilization of Hif1α, which leads to increased glycolysis and lactate release, as well as decreased oxygen consumption. Hif1 abundance can result in *pyruvate dehydrogenase kinase 1* (*Pdk1*) induction, which inhibits pyruvate dehydrogenase (Pdh) via phosphorylation. Therefore, it has been speculated that pyruvate oxidation through Pdh is decreased in pro-inflammatory macrophages. However, to answer this open question, an in-depth analysis of this metabolic branching point was so far lacking. In this work, we applied stable isotope-assisted metabolomics techniques and demonstrate that pyruvate oxidation is maintained in mature pro-inflammatory macrophages. Glucose derived pyruvate is oxidized via Pdh to generate citrate in the mitochondria. Citrate is used for the synthesis of the antimicrobial metabolite itaconate and for lipogenesis. An increased demand for these metabolites decreases citrate oxidation through the TCA cycle, while increased glutamine uptake serves to replenish the TCA cycle. Furthermore, we found that the Pdh flux is maintained by unchanged Pdk1 abundance, despite the presence of Hif1. By pharmacological intervention, we demonstrate that the Pdh flux is an important node for M(LPS) macrophage activation. Therefore, Pdh represents a metabolic intervention point that might become a research target for translational medicine to treat chronic inflammatory diseases.

INTRODUCTION

Macrophages are innate immune cells that differentiate from monocytes, which circulate in the blood stream. Upon differentiation, they invade the surrounding tissue and become resident macrophages (1). Macrophages can be activated by cytokines or toll-like receptor (TLR) agonists, *e.g.* lipopolysaccharide (LPS). In very general terms, macrophage activation can result in rather pro-inflammatory responses, serving as host defense mechanisms or in wound healing responses, aiding in tissue repair and remodelling.

However, depending on the type of activation very different subtypes of activation occur (2). Upon activation with LPS (M(LPS)) or the cytokine interferone-γ (M(Infγ)), macrophages undergo profound metabolic reprogramming, necessary to activate cellular defence mechanisms as well as to cope with different micro-environments in the inflamed tissue (3). A marker for pro-inflammatory activation is high expression of *Irg1* (4,5). We recently showed that *Irg1* codes for the enzyme *cis*-aconitate decarboxylase (Irg1/Cad) that catalyzes the synthesis of the antimicrobial metabolite itaconate from *cis*-aconitate (6). Therefore, metabolic reprogramming due to these adaptations could affect the availability of substrate needed for the synthesis of itaconate during host defense.

The reprogramming during macrophage activation shows overlapping features with cancer cells: both have increased glycolytic rates and increased lactate release, known as aerobic glycolysis or the Warburg effect (7,8). Increased glycolytic rates are observed in any cell type that exceeds the energy demand derived from oxidative phosphorylation (9). In macrophages, it has been revealed that this metabolic rewiring is mediated by stabilization of Hif1α (10). A well-described Hif1 target is *Pyruvate dehydrogenase kinase 1* (*Pdk1)*, an inhibitor of Pyruvate dehydrogenase (Pdh) (11). When Hif1 is stabilized, the Pdh flux can be inhibited by Pdk1 mediated phosphorylation, resulting in decreased pyruvate derived acetyl-CoA levels. In this case, reductive carboxylation of α–ketoglutarate (aKG) increases, to provide sufficient acetyl-CoA for lipogenesis, needed for cell proliferation (12–15). Increased glycolytic rates, decreased Pdh flux and increased reductive carboxylation can also be induced in any cell type when oxygen tension is decreased or when oxidative phosphorylation (OxPhos) is impaired. In this case, NADH oxidation is compromised and citrate levels decrease. This decrease in citrate is linked to an increase in NADH thermodynamically promotes the metabolic adaptation to hypoxia by increasing reductive carboxylation of aKG (13,16,17). However, it is currently unclear if this full panel of metabolic consequences upon Hif1 stabilization is also true for pro-inflammatory macrophages. While it has been demonstrated that Hif1α can be stabilized and activated by cytokines, *e.g.* Tnfα and Il1β (18,19), the detailed metabolic consequences are still uncertain.

Hif1 can bind to the promoter of the *Tlr4* gene, thereby acting through a positive feedback loop on the Tlr4 defense axis (20). Reactive oxygen species were shown to inhibit proteasomal degradation of Hif1α (21) and recently, increased succinate levels in pro-inflammatory macrophages have also been described to stabilize Hif1α, by inhibiting prolyl hydroxylase mediated hydroxylation of Hif1α (10).

In this study, we asked whether the stabilization of Hif1α in M(LPS) macrophages alters TCA cycle fluxes similarly to hypoxic cells. We show that LPS activated macrophages exhibit a metabolic adaptation with overlapping features to hypoxic cells, but also distinct differences, resulting in a unique LPS-specific metabolic signature. The most striking difference to hypoxic cells with stabilized Hif1α is that there is no decrease in relative glucose flux through Pdh, and no increase in reductive carboxylation of aKG. The sustained Pdh flux provides sufficient acetyl-coA for citrate production, which keeps the rate of reductive carboxylation of aKG at a low level, as well as providing citrate that is needed for the synthesis of fatty acids and itaconate. Upon LPS stimulation, high Pdh activity is maintained by a repression of *Pdk1*. As a result Pdh phosphorlylation on ser232 and ser293 remains at low level. Finally, we demonstrate that the Pdh flux is indeed important to sustain M(LPS) activation in macrophages.

EXPERIMENTAL PROCEDURES

Chemicals

UK5099 (Sigma, PZ0160) was first diluted in DMSO and further diluted in medium to a working stock concentration of 10 mM and then spiked into the wells of the culture dish to a final concentration of 100 µM. The final concentration of DMSO did not exceed 1%; LPS (*E.Coli,* Sigma L6529) was prepared as a working stock of 1 µg/ml in glucose and glutamine free DMEM, spiked 1:100 into the wells of the culture dish for a final concentration of 10 ng/ml. Cells were stimulated for 6 hours; Interferon g (mouse) (E.Coli, Sigma I4777) was prepared as a working stock of 5 mg/ml in glucose and glutamine free

DMEM, spiked 1:100 into the wells of the culture dish for a final concentration of 50 ng/ml. Cells were stimulated for 6 hours.

Stable isotope tracing

^{13}C stable isotope tracers were obtained from Eurisotop; Glucose: CLM-1396, Glutamine: CLM-1822-H. The tracer medium was prepared in DMEM without glucose and glutamine. ^{13}C glucose (final 25mM) and ^{12}C glutamine (final 4mM) (or *vice versa*) was added to the medium, pH was set to 7.3, 10 % FBS and 1% P/S were added and finally, the medium was sterile filtered. Tracer medium was prepared in advance and incubated in the hypoxia chamber overnight to remove excessive oxygen from the medium (only for hypoxia conditions). The next morning, medium was replaced by tracer medium and cells were incubated for 24h with the tracer medium to reach isotopic steady state. LPS was added after 24h and left on the cells for an additional 6h prior to extraction. For further information regarding stable-isotope assisted metabolomics see also (22,23).

Cell culture

RAW 264.7 cells (ATCC® TIB-71™) were obtained from ATCC and were cultivated according to the manufacturers instructions. Briefly, cells were kept in DMEM5796 with 10%FBS and 1% P/S at 37°C and 5% CO_2 under atmospheric oxygen concentrations. In the case of hypoxia, cells were cultivated in an incubator at 37°C and 5% CO_2 located in a closed hypoxia chamber with an oxygen concentration of 2%. Cells were simultaneously seeded in the afternoon at a density of 150.000 cells per well in 12-well plates (Thermo Scientific, Nunc Multidish 12 Nunclon Delta Si) and then either incubated either at 21% or 2% O_2 overnight. The next day, medium was replaced. In the case of hypoxia, medium was already incubated in the hypoxia chamber over night to remove excessive oxygen from the medium. For comparison reasons, medium for normoxic conditions was also prepared the day before and incubated in a similar way under atmospheric oxygen conditions. For LPS activation, LPS was added 18h after medium replacement. 24h afer medium replacement cells were harvested.

Viability Assay

To assess cell viability, cells were transferred into tubes and analysed using a Vi-Cell(TM) XR (Beckman Coulter) automated cell counter. To determine viability, cells were incubated with Trypan blue and number of stained cells was determined.

cDNA synthesis and gene expression analysis

cDNA synthesis and qPCR was performed as previously described (Michelucci et al., 2013). Briefly, RNA was isolated from the interphase after extraction of metabolites, using the Qiagen RNAeasy Mini Kit. 0.5 -1 µg RNA was used for cDNA synthesis using SuperScript III (Invitrogen), following the manufacturer's instructions. qPCR was performed using iQ SYBR Green Supermix (Bio-Rad) as per manufacturer's instructions. PCR was carried out on a Light Cycler 480 (Roche). Data analysis was performed using the Roche analysis software according to manufacturer's instructions. Gene expression was normalized to the housekeeping gene L27. For primer sequences, see Table 1.

Extraction of intracellular metabolites

Extraction was according to (24). Briefly, cells were cultivated in 12-well plates and washed with 1 ml of 0.9% NaCl and quenched with 0.2 ml -20 °C methanol. After adding an equal volume of 4 °C cold water, cells were collected with a cell scraper and transferred to tubes containing 0.2 ml -20 °C chloroform. The extracts were shaken at 1400 rpm for 20 min at 4 °C (Thermomixer Eppendorf) and centrifuged at 16,000×g for 5 min at 4 °C. 0.2 ml of the upper aqueous phase was collected in specific glass vials with micro inserts and evaporated under vacuum at -4°C using a refrigerated CentriVap Concentrator (Labconco).

Gas Chromatography-Mass Spectrometry

Metabolite derivatization was performed using a Gerstel MPS. Dried polar metabolites were dissolved in 15 µl of 2% methoxyamine hydrochloride in pyridine at 40 °C under shaking. After 60 min, an equal volume of MTBSTFA was added and held for 60 min at 40°C. 1 µl of sample was injected into an SSL injector at 270°C in splitless mode. GC/MS analysis was performed using an Agilent 7890A GC equipped with a 30m DB-35MS + 5m Duraguard capillary column. Helium was used as carrier gas at a flow rate of 1.0 ml/min. The GC oven temperature was held at

100 °C for 2 min and increased to 300 °C at 10 °C/min. After 3 min, the temperature was increased to 325 °C. The GC was connected to an Agilent 5975C inert XL MSD, operating under electron ionization at 70 eV. The MS source was held at 230 °C and the quadrupole at 150 °C. The MS was operated in selected ion monitoring (SIM). The total run time of one sample was 25.00 min. All GC/MS chromatograms were processed by using MetaboliteDetector software (25). MIDs were determined and corrected for natural isotope abundance using MetaboliteDetector.

Measurement of glucose and lactate intensities was performed by derivatization with an equal volume of MSTFA (instead of MTBSTFA) and held for 30 min at 40 °C under continuous shaking. 1 µl sample was injected into an SSL injector at 270°C in split 10 mode. GC oven temperature was held at 90°C for 1 min and increased to 300 °C at 15 °C/min for 8 min to 320°C. The total run time of one sample was 24.3 min. For absolute quantification of glucose and lactate, a dilution series of a standard mix was included in the sequence and measured in triplicates. For normalization, we used [U-^{13}C]glucose and [U-^{13}C]lactate as internal standards (in this case, medium samples contained only ^{12}C carbon sources).

Quantification of Amino Acids

Quantification of amino acids was performed on an Agilent 1100 HPLC System equipped with a Diode Array Detector. Separation was carried out on a ZORBAX Amino Acid Analysis Column (150 x 4.6 mm, 5µm) with a preceding ZORBAX Amino Acid Analysis Guard Cartridge (Agilent Technologies, Santa Clara, CA, USA) at 40°C in gradient mode (see Table 1). The eluents used were 40 mM Na_2HPO_4 (pH 7.8, eluent A) and a mixture of Acetonitrile, Methanol and Water (45:45:10, eluent B). 0.02% sodium azide was added to eluent A to prevent microbial growth. Primary amines were automatically derivatized with ortho-phthalaldehyde (OPA) in borate buffer (0.4 N in water, pH 10.2) and diluted in eluent A prior to injection. The resulting OPA-derivatives were subsequently detected at 338 nm (10 nm bandwidth – reference wavelength: 390 nm, 20 nm bandwidth). All medium samples were diluted 1:1 with the internal standard L-2-aminobutyric acid (final concentration: 300 µM) to correct for deviations resulting from the derivatization-process. External calibration standards as well as reference media with known concentrations were measured with every run to determine sample concentrations and ensure stability of the analysis. Gradient profile: 1.9 min: 0 % eluent B; 18.1 min: 57 % eluent B; 18.6 min: 100 % eluent B; 22.3 min: 100 % eluent B; 23.2 min: 0 % eluent B; 26 min: 0% eluent B.

Western Blot

For preparation of whole cell extract, 1x10^6 cells were harvested, washed with ice cold 1x phosphate buffered saline (PBS) (Invitrogen/Life Technologies Europe BV Belgium), lyzed in 1x M-PER®, Mammalian Protein Extraction Reagent (Thermo Scientific, Belgium) completed with 1x protease inhibitor cocktail (Complete®, Roche, Luxembourg) and further processed according to manufactures instructions. A Nanodrop analyzer was used to measure the protein concentration. Proteins were separated by size using SDS-PAGE (12%) and transferred to an Immobilon-FL PVDF membrane (Merck Millipore) using the Mini-PROTEAN Tetra Cell and PowerPac Basic Power Supply (Bio-Rad, Belgium). The membrane was blocked in 5 % non-fat milk powder in PBS-Tween for 1 h at room temperature or over night at 4°C. Used antibodies: Anti-Irg1 (Sigma, hpa040143) 1:750 in PBS-T 5% non-fat milk powder for 1 h at room temperature; Anti-PDK1 (rabbit): (Enzo #ADI-KAP-PK112) 1:3000 in TBST 5% BSA, o/n at 4°C; Anti-PDH-E1alpha (rabbit) (pSer232) (Millipore #AP1063) 1:1000 in TBST 5% BSA, o/n at 4°C; Anti-PDH-E1alpha (rabbit) (pSer300) (Millipore #ABS194) 1:1000 in TBST 5% BSA, o/n at 4°C; Anti-PDH-E1alpha (rabbit) (pSer293) (Millipore #ABS204) 1:10000 in TBST 5% BSA, o/n at 4°C; Anti-alpha-tubulin (mouse) 1:5000 in TBST 5% BSA, o/n at 4°C; anti-rabbit-HRP 1:5000 in TBST 5% Skim Milk (Cell signalling); anti-mouse-HRP 1:5000 in TBST 5% Skim Milk (Cell signalling). Visualization was done using the ECL Plus Western Blotting Detection System Kit (GE Healthcare, Netherlands). Signals were detected using the LI-COR System. Quantification of band intensities was done using the ImageStudioLite Software package.

Cell imaging and data analysis

Phase contrat images were acquired using a 10X objective on a Nikon Ti Eclipse inverted microscope with motorized stage (Nikon Corporation, Tokyo, Japan) enclosed in a bench top incubator. Automatic microscope control, stage programming and acquisition were done using the OptoMorph version of MetaMorph 7.8.10 (Cairn Research, Kent, UK). LPS treated and untreated RAW 264.7 cells growing in 12-well Nunc plates (50.000 cells per well) were imaged in positive phase contrast. Nine adjacent but non-overlapping images were automatically acquired in a 3x3 grid around the center of each well. The entire imaging experiment was performed twice, resulting in 36 images acquired per condition. One out-of-focus image and five containing cell aggregates were excluded from further analysis. Surfaces of strongly attached cells were estimated by thresholding in ImageJ 2.0.0-rc-31/1.49v using the IJ_IsoData algorithm. Congruence of thresholding results with cell contours was verified by visual inspection. Cell sizes were calculated using the particle analysis tool, allowing for areas from 50 to 5000 px and excluding particles on the image edges. Average sizes were reported for each image. Halo and contrast effects resulting from the phase-contrast imaging were analyzed to discriminate between strongly and weakly attached cells. Strongly attached cells appeared darker than background with weak halo, while weakly attached cells appeared brighter than background with strong halo. Histograms of pixel intensities of the entire field of view were analyzed using custom software written in MATLAB R2014b. First, the intensity peak corresponding to the background signal (cell-free surface) was identified and approximated by a Gaussian function. The approximated peak was subtracted from the original histogram and the weighted sum of intensities below (dark) and above (bright) the background peak was calculated, respectively. The ratio of dark-to-bright values informs on the ratio of strongly-to-weakly attached cells. Renormalization of this ratio by values obtained for individual strongly and weakly attached cells yielded an adhesion index with values from 0 (no cells attached) to 1 (all cells attached).

Statistical analyses

To analyze a significant difference between two groups, unpaired Welch's *t*-Test was applied. p – values are indicated in each panel (* $p < 0.01$; or as indicated) and was considered as significant different with a p – value < 0.05. The number of independent replicates is indicated in the figure legends. Each experiment was at least performed three times with cells of a different passage. Each individual experiment consisted of three wells per condition.

RESULTS

M(LPS) macrophages show a distinct metabolite signature

The macrophage environment is likely to be hypoxic, as these cells infiltrate hypoxic tissues such as tumors, wounded regions or sites of inflammation. At the site of inflammation, different oxygen tensions result from increased oxygen demand as well as swelling or vascular damage (26,27). To physiologically meet these challenging conditions, macrophages are well adapted to hypoxia by their ability to adjust their gene expression profile and increase glycolytic activity (28). To study if the activation of macrophages reprograms metabolism to a hypoxia-like phenotype, we cultivated the murine macrophage cell line RAW 264.7 under normoxia (21% oxygen) and hypoxia (2%) and activated it with LPS for 6h. We selected this time point, because it reflects the highest expression level of *Irg1*, the gene that codes for the enzyme which catalysis the synthesis itaconate (6).

We analysed intracellular metabolite levels and revealed that LPS stimulation resulted in increased levels of itaconate, succinate and lactate under normoxia (Figure 1A-C). These three metabolites are marker metabolites for M(LPS) activation, demonstrating a clear pro-inflammatory activation (6,10,29,30). Moreover, we observed increased levels of the TCA cycle associated metabolites malate and glutamate, whereas aspartate and citrate levels remained unchanged (Figure 1D-G). The amino acids glycine, serine and alanine were also elevated upon LPS stimulation (Figure 1H-J). Compared to normoxia, LPS treatment of hypoxic cells was unable to induce similar itaconate and succinate levels (Figure 1A and B). As expected,

lactate levels further increased upon hypoxia as a result of reduced respiration and concomitant increased glycolysis, known as the Pasteur Effect. Non-activated, hypoxic cells exhibited decreased levels of the TCA cycle associated metabolites malate, aspartate, glutamate and citrate. However, LPS stimulation under hypoxia resulted in increased levels of malate, aspartate and glutamate but not citrate (Figure 1D-G). The amino acids, glycine and serine were unchanged between hypoxia and normoxia. Upon LPS activation of hypoxic cells, serine and alanine were increased (Figure 1H-J). Interestingly, we also observed a trend of increased levels of the branched chain amino acids isoleucine, leucine and valine under hypoxia for both non-stimulated and LPS stimulated conditions (Figure 1K; p-value > 0.05).
We concluded from these results that LPS affects the metabolite profile of macrophages independent of the oxygen supply and that this profile is clearly different to a pure hypoxic profile. Intriguingly, we observed decreased abundance of the antimicrobial metabolite itaconate under oxygen limiting conditions, which could have direct effects on the immune response in tissues with low oxygen tension.

Decreased itaconate levels under hypoxia are not the result of decreased *Irg1* expression or lower Irg1/Cad protein abundance

To investigate if the reduced levels of itaconate are caused by transcriptional repression, post-transcriptional regulation or post-translational regulation, we analyzed gene expression and protein levels of the catalyzing enzyme Irg1/Cad. We found that hypoxia does not significantly reduce the gene expression level or the protein abundance of Irg1/Cad, indicating a regulation at the post-translational level or a result of decreased substrate concentrations (Figure 2A and B). To confirm LPS activation of macrophages, we analyzed gene expression of the pro-inflammatory marker genes *Tnfα, iNos* and *Il1β* (Figure 2C-E). We found clear up-regulation under both oxygen conditions when the cells were treated with LPS. However, hypoxia resulted in a 20 % reduction of *Tnfα* expression and approximately three-fold higher expression of *Il1β* and *iNos*.
It has been reported in several recent publications that Hif1α gets stabilized in M(LPS) macrophages compared to resting macrophages (10,21,29,31). Therefore, we also analyzed gene expression of *Hif1α*, and we observed increased expression of *Hif1α* in response to LPS treatment under hypoxia (Figure 2F), indicating that Hif1α stabilization in hypoxic M(LPS) macrophages can be a combined effect of increased transcriptional expression and post-translational stabilization. Under normoxia, no difference in *Hif1α* expression was detected.
Based on these results we conclude that the reduction of itaconate under hypoxia is mostly a result of post-translational effects such as altered metabolic fluxes, either due to an enzyme modification that regulates its activity or by changing substrate concentrations. To that end, we were interested to compare cellular flux changes with LPS activation between hypoxia and normoxia.

LPS activation promotes pyruvate oxidation via Pdh by preventing *Pdk1* expression

To monitor intracellular glucose derived fluxes in M(LPS) macrophages, we incubated RAW264 cells for 24h in the presence of uniformly labeled [U-^{13}C]glucose to reach isotopic steady state conditions. During these 24h, labeled glucose is metabolised within the cells and is incorporated in cellular metabolites downstream of glucose. To obtain the specific labeling patterns, intracellular metabolites were extracted and analyzed with gas chromatography/mass spectrometry to determine mass isotopomer distributions (MIDs; corrected for natural isotope abundance), which reflect relative metabolic fluxes (Figure 3A for atom transitions) (22,23).
As expected, stable isotope labeling revealed that hypoxia resulted in decreased pyruvate flux through Pdh, illustrated by decreased M2 citrate isotopologues (Figure 3B). Concomitant with decreasing citrate M2 isotopologues under hypoxia, we observed increased abundance of citrate M0 isotopologues, representing citrate molecules derived from carbon sources other than glucose (Figure 3B). This decrease is a result of Hif1α stabilization and *Pdk1* induction, which inhibits Pdh by phosphorylation (32,33). Decreased pyruvate oxidation under hypoxia promotes decreasing downstream substrate levels,

most probably resulting in the observed decreased itaconate levels (Figure 1A). However, Hif1α has also been shown to be stabilized in M(LPS) macrophages under normoxic conditions (10,29). Therefore, it is speculated that pyruvate oxidation through Pdh is decreased in M(LPS) macrophages, a similar phenotype to cancer cells with stabilized Hif1α (3,34). However, we did not observe decreased citrate M2 isotopologues in normoxic M(LPS) macrophages, raising the question if Pdh is inhibited under these conditions.

To analyse regulation of Pdk1 in more detail we investigated gene expression and protein abundance of Pdk1 and phosphorylation status of Pdh (Figure 3C-H). In line with current knowledge, hypoxia mediated stabilization of Hif1α resulted in increased *Pdk1* expression (Figure 3C), which complements our observation of hypoxia-dependent, decreased glucose flux to citrate (Figure 3B). Intriguingly, we observed that LPS stimulation resulted in a drastic reduction of *Pdk1* expression at both normoxia and hypoxia, indicating that Pdk1 mediated inhibition of Pdh is reduced in M(LPS) macrophages (Figure 3C). Moreover, analysis of Pdk1 protein abundance revealed similar Pdk1 levels in non-activated or M(LPS) activated macrophages. Only in hypoxia did we observe a significant increase of Pdk1 abundance (Figure 3D,E). To investigate if the low levels of Pdk1 have an effect on Pdh, we analyzed phosphorylation of Pdh on serine 232, 293 and 300 (Figure 3 D, F-H). Phosphorylation of these residues has been reported to result in an inhibition of Pdh activity (33). As expected, hypoxia resulted in increased phosphorylation of the three analyzed serine residues (not significant in case of Ser300). However, and in line with low Pdk1 levels in normoxic M(LPS) macrophages, LPS activation did not increase phosphorylation levels of Ser 232 and 293. Regarding Ser 300, we observed significantly increased phosphorylation upon LPS activation while there was no further significantly increased phosphorylation due to hypoxia. If Ser300 specifically has a unique function in the context of LPS activation in macrophages remains to be determined in future work. Our results from this part of the study reveal that Hif1 mediated induction of *Pdk1* can be attenuated by LPS stimulation, which is in line with increased citrate M2 isotopologues upon LPS activation (Figure 3B).

In line with the results of Pdk1 abundance and Pdh phosphorylation status, our stable isotope analysis revealed that LPS stimulation did not result in a decreased relative pyruvate oxidation, both under hypoxia and normoxia (Figure 3B and I), indicating that Hif1 did not mediate Pdh inhibition upon LPS stimulation. We observed increased citrate M2 isotopologue levels, reflecting even higher relative pyruvate flux through Pdh (Figure 3B). To normalize for upstream changes in glycolysis, we determined the ratio of M2 citrate/M3 pyruvate and observed an increase upon LPS stimulation, indicating increased pyruvate flux through Pdh in M(LPS) macrophages (Figure 3I). As a reduction of citrate M2 isotopologues was only observed under hypoxic conditions, Hif1 mediated inhibition of Pdh depends only on the oxygen tension and not on the macrophage activation status. Indeed, LPS activation can even partially recover the Hif1 mediated Pdh inhibition under hypoxia (Figure 3B and I).

The M2 abundance of aKG and malate were significantly lower than in citrate (Figure 3J and K), suggesting that large amounts of citrate, *cis*-aconitate or isocitrate are either used for pathways other than the oxidative TCA cycle, or that other carbon sources (e.g. glutamine) increase their contribution to aKG and malate. Stimulation with LPS as well as hypoxia further decreased glucose contribution to aKG and malate, as can be seen by a decreasing abundance of aKG and malate M2 isotopologues (Figure 3J and K).

Next, we analyzed glucose uptake from the medium and cellular lactate release, to evaluate if M(LPS) macrophages increase their glycolytic rate. Under normoxia, LPS stimulated macrophages increased glucose uptake and lactate release whereas under hypoxia, glucose uptake and lactate release were exceeding the rate of M(LPS) macrophages under normoxia (Figure 3L). This effect was further enhanced when hypoxic cells were additionally stimulated with LPS (Figure 3L). Under normoxia, the lactate to glucose ratio was increased from 1.2 to 1.6 upon LPS stimulation, indicating increased activity of LDH, which is in line with the Warburg-like phenotype of M(LPS) macrophages (3). However,

20% of the overall glucose carbon pool is still available for other metabolic pathways, indicating that M(LPS) macrophages still contain sufficient pyruvate to maintain oxidation through Pdh.

It has been shown before that Stat3 specific signaling can inhibit Pdh and thus block pyruvate oxidation through Pdh in primary fibroblasts and cancer cell lines (35). Therefore we investigated if, and in contrast to LPS treatment, a Stat3 dependent activation with the cytokine interferon-γ (Infγ) might inhibit Pdh. To this end, we treated the cells with Infγ or LPS and analyzed the isotope enrichment in citrate. We did not observe a difference between LPS and Infγ treatment (Figure 3M). In both cases, M2 citrate was significantly increased compared to untreated controls. In line with LPS activation we also observed decreased expression of *Pdk1* in M(Infγ) macrophages (Figure 3N), indicating no inhibition of pyruvate oxidation in M(Infγ) macrophages. In conclusion, sustained pyruvate flux through Pdh and its regulation by Pdk1 seems to be independent of Tlr4 signalling.

LPS activation increases glutamine uptake but does not induce reductive carboxylation of aKG

It has been demonstrated that hypoxic cells metabolize increased amounts of glutamine via reverse IDH activity to generate citrate by reductive carboxylation of aKG (12–15) This pathway fuels the citrate pool to provide sufficient acetyl-coA for lipogenesis. Since M(LPS) activation also results in a stabilization of Hif1α (10,19,21,29) and increased glycolytic flux (see Figure 3I and L), we investigated if these cells exhibit increased reductive carboxylation of aKG. To that end, we applied a uniformly labeled [U-^{13}C]glutamine tracer and determined MIDs of TCA cycle metabolites (Figure 4A for atom transitions).

As expected, under hypoxic conditions we observed a drop in oxidative TCA cycle activity and a strong induction of reductive carboxylation, inferred from decreased citrate M4 and increased citrate M5 isotopologues (Figure 4B-D). This pattern was also reflected by decreasing malate M4 (oxidative route) and increasing malate M3 (reductive route) isotopologues (Figure 4E). However, when cells were stimulated with LPS at normoxic conditions, reductive carboxylation of aKG was not increased (Figure 4D).

Using the glutamine tracer, we observed that the major carbon source of aKG was glutamine, and that upon LPS stimulation and under hypoxia, the abundance of M5 isotopologues increased, suggesting an increase in glutamine influx and a decreasing glucose contribution (Figure 4F). While hypoxia results in increased usage of aKG for reductive carboxylation and decreased aKG oxidation (14,15), we did not find evidence that LPS stimulation under normoxia compromises the relative glutamine carbon flux through aKG dehydrogenase, indicated by a similar enrichment pattern of aKG and malate.

To analyze glutamine metabolism more in detail, we quantified glutamine uptake from the medium and glutamate release from the cells. While hypoxia did not result in increased glutamine uptake, we observed a strong increase of glutamine uptake upon LPS stimulation under both oxygen levels (Figure 4G). Since glutamate is produced from glutamine and can be released from the cell, we quantified glutamate release to infer glutamine anaplerosis to the TCA cycle. Although we observed increased glutamate release upon LPS stimulation, the net uptake of glutamine in LPS stimulated cells was still higher compared to untreated controls (ctrl: 12.84 *vs* LPS: 20.5 fmol/cell/h) (Figure 4G and H). As indicated by the intracellular metabolite levels (Figure 1K), we also observed a trend of increased consumption of branched chain amino acids from the medium upon LPS stimulation (Figure 4I). However, these differences were only significant in the case of leucine. Nevertheless, we believe that the influence of branched chain amino acids on central metabolism is higher upon LPS activation.

To better understand the impact of the different carbon sources to the TCA cycle metabolites, we calculated the carbon contributions of glucose and glutamine to citrate, aKG, malate and itaconate (Figure 4J). We observed a small decrease in glucose contribution to citrate upon LPS activation. However, based on the [U-^{13}C]glucose derived MIDs, this decrease mostly originated from decreased citrate cycling through the oxidative TCA cycle (compare M3, M4 and M5 isotopologues in Figure 3B) or increased

glutamine influx, rather than decreased pyruvate flux through Pdh (M2 isotopologue). Hypoxia resulted in a stronger reduction of glucose contribution to citrate, which was a result of Pdh inhibition. Along with the decrease in glucose contribution, the glutamine contribution to citrate was increased upon LPS, especially under hypoxia, where glutamine is the major carbon source of citrate. For aKG and malate, the glucose contribution was significantly lower compared to citrate, indicating that major parts of the citrate pool are not used for further oxidation through the oxidative TCA cycle, but for anabolic processes such as lipid synthesis or itaconate synthesis. In line with this observation we observed higher glucose contribution to itaconate, compared to aKG and malate. Moreover, upon LPS stimulation, and especially with hypoxia, we observed an increase of other carbon sources than glucose or glutamine, which is in line with potentially increased uptake of branched chain amino acids (Figure 1K and 4I).

In summary, we observed that glutamine is the major carbon source of the TCA cycle in M(LPS) macrophages and is the main substrate for TCA oxidation. Glucose carbon still enters the cycle at citrate, however significant amounts of the citrate pool are not further oxidized through IDH but are distributed to other metabolic pathways. Glutamine serves to replenish this lack of carbon by increased uptake upon LPS stimulation.

LPS causes an increase in lipogenesis in RAW264 cells

Besides transcriptional and metabolic adaptations to inflammation, it has been described that pro-inflammatory macrophages also undergo morphological changes from small and spherical to a larger and more attached form (Figure 5A). To demonstrate the surface enlargement during LPS activation, we monitored cell size by using two orthogonal microscopy approaches (Figure 5B), demonstrating an increase in cell surface and thus pointing to an increased demand on lipids needed for membrane formation. Furthermore, M(LPS) macrophages increase intracellular and extracellular vesicle formation during pathogen defense (36). Therefore, M(LPS) macrophages have an increased demand for lipids, needed for morphological changes and vesicle formation. To meet this demand, LPS activated macrophages need to prioritize their metabolism towards lipogenesis and to repress lipid oxidation. In line with this necessary metabolic shift, we observed decreased expression of *carnitine palmitoyltransferase 1* (*Cpt1*), which imports palmitate into the mitochondrion for lipid oxidation and subsequent energy production (Figure 5C). A reduction of ß-oxidation is in line with reports of decreased oxidative metabolism in M(LPS) macrophages (37) and supports the observed increased demand for lipids. High activity of lipid degradation, simultaneously to their synthesis, would be a waste of energy.

To generate lipids from central metabolism, cells export mitochondrial citrate into the cytoplasm where it is hydrolyzed via ATP dependent citrate lyase (Acly) to provide acetyl-coA for lipogenesis. In this preferred case, citrate utilization is for anabolic processes rather than the TCA cycle. To analyze the contribution of glucose and glutamine to palmitate, an endpoint of fatty acid synthesis, we determined the MIDs of - and carbon contributions to - palmitate after both the application of [U-^{13}C]glucose and [U-^{13}C]glutamine as tracers in independent experiments (Figure 5D and E). We observed that under normoxia, nearly 50% of the carbon in palmitate originated from glucose. Under hypoxic conditions, a shift in isotopologues indicated that the glucose contribution was reduced while glutamine contribution was increased, suggesting increased reductive carboxylation under hypoxia, but not as a result of LPS stimulation. Although dependent on the pool sizes of the metabolites, increased production of itaconate and palmitate from glucose derived citrate in M(LPS) macrophages indicates reduced citrate oxidation through the TCA cycle in M(LPS) macrophages.

Pyruvate flux to citrate is important for LPS activation in RAW264 cells

To investigate the importance of the Pdh flux in M(LPS) macrophages, we used a pharmacological approach to impair pyruvate oxidation through Pdh by inhibiting the pyruvate transporter with the specific inhibitor UK5099 (38). Using this inhibitor together with the [U-^{13}C]glucose tracer,

we observed a significant decrease of citrate M2 isotopologues, indicating reduced relative pyruvate oxidation through Pdh (Figure 6A). Addition of LPS to UK5099 treated cells could not restore the abundance of M2 citrate, since pyruvate supply is impaired by the inhibition of the transporter. Analysis of intracellular metabolite levels revealed that inhibition of pyruvate transport into the mitochondrion resulted in decreased amounts of citrate, originating from reduced substrate levels for citrate synthase (Figure 6B). Intriguingly, we also observed decreased amounts of the inflammatory marker metabolites itaconate and succinate under pro-inflammatory conditions (Figure 6C and D). Decreased amounts of itaconate and succinate could either result from decreased glucose flux into the TCA cycle, similar to hypoxia, or from a metabolic alteration in M(LPS) macrophages. To analyze these hypotheses, we investigated the gene expression profiles of pro-inflammatory marker genes (Figure 6E-H). While, *Il1b* gene expression was not significantly decreased (Figure 6E), we observed that UK5099 treatment of LPS stimulated macrophages resulted in decreased expression levels of *iNos*, *Irg1* and *Tnfα* (Figure 6F-H), indicating that in this case and in contrast to hypoxia, the observed decreased itaconate level roots back to decreased *Irg1* levels. Moreover, application of UK5099 to LPS stimulated cells resulted in increased *Cpt1* expression levels, similar to untreated controls, while *Pdk1* expression was still reduced, due to the fact that pyruvate import into the mitochondrion was inhibited, and thus regulation of Pdh not necessary (Figure 6I and J). To exclude a potential toxic effect of UK5099 on RAW264 cells, we performed a viability assay and did not observe significant changes in viability (Figure 6K). To further exclude the possibility of timing effects due to simultaneous addition of LPS and UK5099, we repeated the experiments with a modified experimental setup, where we first activated the cells with LPS for 3h and added then UK5099 for additional 6h to investigate if this intervention can repress the pro-inflammatory profile of M(LPS) macrophages (Figure 6L). Following this approach we also observed significantly decreased citrate, itaconate and succinate levels (Figure 6M-O) and significantly decreased expression of *Tnfα, iNos*, *Irg1* and *Il1b* (Figure 6P-S). These results indicate that inhibition of pyruvate import into the mitochondrion can indeed supress pro-inflammatory responses in M(LPS) macrophages. Finally, we investigated the effect of carbon contribution to palmitate for these conditions, using [U-^{13}C]glucose as a tracer, in combination with UK5099. In line with decreased citrate, itaconate and succinate levels upon UK5099 treatment, we also observed lower carbon contribution from glucose to palmitate (Figure T and U).

In summary, these data demonstrate that the pyruvate flux through Pdh is important for LPS activation in macrophages. Apparently, altered metabolic fluxes or changes in metabolite concentrations enable a feedback mechanism to regulate cellular gene expression profiles. Hence, metabolic intervention can be used to attenuate activation of M(LPS) macrophages.

DISCUSSION

M(LPS) macrophages require extensive reprogramming to enable host defense mechanisms. While M(IL4) macrophages increase oxidative metabolism optimized for tissue repair (39), M(LPS) macrophages develop a Warburg-like phenotype by increasing glycolysis and lactate release (3). It has been demonstrated that pro-inflammatory activation results in the stabilization of Hif1α, Hif1 complex formation with monomeric or dimeric PKM2, along with an increased expression of M(LPS) associated cytokines and bacterial defense mechanisms (29). Since, under hypoxia, Hif1 not only increases the glycolytic activity, but also represses Pdh activity through Pdk1, it was speculated that glucose flux through Pdh is also repressed in M(LPS) macrophages (3,40). However, this would withdraw carbon supply, necessary for lipogenesis and synthesis of the antimicrobial metabolite itaconate.

In this work, we demonstrate that the Pdh flux plays an important role in maintaining full LPS specific activation and that pharmacological intervention to prevent pyruvate oxidation represses pro-inflammatory activation. Although an active Pdh flux has been speculated for early

macrophage differentiation and for dendritic cells before (3,41), our results demonstrate that pyruvate oxidation through Pdh is fully active in mature M(LPS) macrophages and that this is even essential to sustain LPS activation. Moreover, we discovered that this process is facilitated by repressed *Pdk1* expression and no increase in Pdk1 protein abundance, as well as significantly lower phosphorylation of Pdh compared to hypoxic conditions, illustrating that M(LPS) macrophages sustain an active pyruvate flux through Pdh.

Under hypoxia, Hif1 decreases pyruvate oxidation through Pdh by inducing *Pdk1* (32). In contrast to hypoxia, we demonstrated that although glycolysis is increased and oxygen consumption is decreased (29) in M(LPS) macrophages, pyruvate oxidation through Pdh is not inhibited, because Pdk1 abundance is not increased. Active Pdh facilitates a stable citrate pool, which in turn prevents increased reductive carboxylation of aKG by thermodynamic means (16). M(LPS) macrophages have been shown to increase their expression of the mitochondrial citrate carrier to transport citrate from the mitochondrion into the cytosol (42) and we have shown that M(LPS) macrophages have an increased lipid demand. Since we demonstrated that reductive carboxylation of aKG is not increased, the high demand of citrate has to be mostly supplied by glucose through Pdh.

When Pdh flux is repressed, citrate is increasingly generated by reductive carboxylation of aKG, which is mostly derived from glutamine (43). An increased demand on glutamine in M(LPS) macrophages has been reported before (44). Here we describe in detail how this glutamine is utilized. In M(LPS) macrophages most glutamine is preferentially used for glutaminolysis rather than for reductive carboxylation of aKG. Besides Acly derived oxaloacetate, increased glutaminolysis additionally provides oxaloacetate, which is needed as an acceptor for pyruvate derived acetyl-coA and the synthesis of citrate. It also replenishes the TCA cycle to compensate for increased lipogenesis and the loss of carbon that is used for the synthesis of itaconate.

It is known that LPS activation results in decreased oxygen consumption, which suggests that TCA cycle activity is decreased and would provide less NADH to be oxidized via the ETC (29,45,46). However, we found evidence that the oxidative TCA cycle is still running and is fueled by increased amounts of glutamine. TCA cycle derived NADH can be used for alternative routes and would consequently not be oxidized via the ETC and thus, also result in reduced oxygen consumption rates. Mitochondrial derived NADH can alternatively be converted to NADPH by nicotinamide nucleotide transhydrogenase (17,47), which is utilized by M(LPS) macrophages for ROS production via NADPH oxidase, needed for antibacterial activity (48), or transferred to the cytoplasm (49) where it is needed for lipogenesis. Therefore it is possible that M(LPS) macrophages use increased amounts of TCA cycle derived NADH for the generation of NADPH rather than oxidizing it via the ETC, which fits to the reported decreased oxygen consumption rates (6,45,46). Additionally, the ETC can be directly inhibited by nitrosylation (50,51) promoted by increased expression of *iNos*, which we have shown to be increased upon LPS stimulation. Therefore, decreased oxygen consumption in M(LPS) macrophages due to decreased ETC activity is reasonable, but a decreased ETC activity does not necessarily have to result in decreased oxidative TCA cycle activity.

Although we could demonstrate that Pdh activity is important in M(LPS) macrophages, the mechanism of how *Pdk1* repression is facilitated despite the presence of Hif1 needs additional research. One possibility would be a weaker stabilization because Hif1α is not as abundant as in hypoxic cells. However, in this case we would still expect a similar mode of action, and therefore, a moderate induction of *Pdk1*. LPS activation exhibits distinct regulatory modules (2) and we conclude that these specific networks overlap with the classical Hif1 signature to mediate LPS specific activation. Since we demonstrated that M(LPS) macrophages depend on the Pdh flux to induce cytokine expression and synthesis of itaconate, it appears that a specific Hif1 induced upstream regulator exists which specifically prevents *Pdk1* expression. In this way, increased glucose uptake and lactate release can still be facilitated by Hif1, whereas Pdk1 activity is prevented by an additional regulator. Overall, this points towards a context-dependent Hif1 response.

With the hypoxia model, we demonstrated that the decreased pyruvate flux through Pdh results in decreased levels of the antimicrobial metabolite itaconate as well as decreased levels of succinate. However, gene expression of *Irg1* was unchanged. We conclude that, under hypoxia, decreased metabolite levels are a passive effect of decreased pyruvate oxidation and decreased oxidative mitochondrial metabolism. This also illustrates that Hif1 mediated inhibition of Pdh would be disadvantageous to M(LPS) macrophages and that parts of the TCA cycle are indeed important for M(LPS) macrophages *e.g.* for the synthesis of lipids and itaconate.

By inhibiting the pyruvate import into the mitochondria of M(LPS) macrophages, we observed decreased metabolite levels of itaconate and succinate, similar to hypoxia. Intriguingly, in the case of transport inhibition, gene expression of *Irg1, Tnfα* and *iNos* were decreased as well. All of these genes are hallmarks of LPS activation, indicating a general impairment of activation in matured M(LPS) macrophages.

Based on our observations we can now extend the existing metabolic model of M(LPS) macrophages (Figure 7): (1) We confirmed the findings of increased glycolysis and increased lactate release, (2) Furthermore, reductive carboxylation of aKG is not increased in M(LPS) macrophages, but instead glutamine is still oxidized through aKG dehydrogenase, (3) Lastly, pyruvate is still oxidized through Pdh, which turned out to be essential for full LPS activation. Our work revealed a LPS specific metabolic feature that is essential for activation and that might be approached by further studies in the light of translational medicine, to develop novel therapies against inflammatory dysfunctions.

Acknowledgments: Related research of the authors was supported by the Fonds National de la Recherche (FNR) Luxembourg (ATTRACT A10/03 (Hiller) and AFR-Postdoc-3973022 (Meiser)). SCS acknowledges financial support from the HICE Virtual Institute. JM thanks Dr. Daniel Weindl and Dr. Andre Wegner from the Metabolomics group for fruitful discussions. We thank Yannic Nonnenmacher from the Metabolomics group for technical assistance with the HPLC. We thank Dr. Aidos Baumuratov from the LCSB Imaging Facility for assistance and technical support with the microscopes.

Conflict of interest: The authors declare that they have no conflicts of interest with the contents of this article.

Author Contributions: JM designed the concept of this work, performed experiments, analyzed data and wrote the manuscript. LK performed experiments and analyzed data. SCS performed experiments, analyzed data and revised the manuscript. NB and JG performed western Blots. AF and AS did the microscopy analysis. KH discussed experiments and revised the manuscript. All authors read and agreed to the content of this manuscript.

REFERENCES

1. Gordon S, Taylor PR. Monocyte and macrophage heterogeneity. Nat Rev Immunol. 2005 Dec;5(12):953–64.

2. Murray PJ, Allen JE, Biswas SK, Fisher EA, Gilroy DW, Goerdt S, et al. Macrophage activation and polarization: nomenclature and experimental guidelines. Immunity. 2014 Jul 17;41(1):14.

3. Kelly B, O'Neill LA. Metabolic reprogramming in macrophages and dendritic cells in innate immunity. Cell Res. 2015 Jun; Available from: http://www.nature.com/doifinder/10.1038/cr.2015.68

4. Basler T. Mycobacterium paratuberculosis, Mycobacterium smegmatis, and lipopolysaccharide induce different transcriptional and post-transcriptional regulation of the IRG1 gene in murine macrophages. J Leukoc Biol. 2005 Dec;79(3):628–38.

5. Degrandi. The proinflammatory cytokine-induced IRG1 protein associates with mitochondria. 2009;29(1):55–68.

6. Michelucci A, Cordes T, Ghelfi J, Pailot A, Reiling N, Goldmann O, et al. Immune-responsive gene 1 protein links metabolism to immunity by catalyzing itaconic acid production. Proc Natl Acad Sci. 2013 May;110(19):7820–5.

7. Warburg O. Über den stoffwechsel der carcinomzelle. Naturwissenschaften. 1924;12(50):1131–7.

8. Warburg O, others. On the origin of cancer cells. Science. 1956;123(3191):309–14.

9. Vazquez A, Liu J, Zhou Y, Oltvai ZN. Catabolic efficiency of aerobic glycolysis: the Warburg effect revisited. BMC Syst Biol. 2010;4:58.

10. Tannahill GM, Curtis AM, Adamik J, Palsson-McDermott EM, McGettrick AF, Goel G, et al. Succinate is an inflammatory signal that induces IL-1β through HIF-1α. Nature. 2013 Mar;496(7444):238–42.

11. Denko NC. Hypoxia, HIF1 and glucose metabolism in the solid tumour. Nat Rev Cancer. 2008;8(9):705–13.

12. Filipp FV, Scott DA, Ronai ZA, Osterman AL, Smith JW. Reverse TCA cycle flux through isocitrate dehydrogenases 1 and 2 is required for lipogenesis in hypoxic melanoma cells. Pigment Cell Melanoma Res. 2012;25(3):375–83.

13. Mullen AR, Wheaton WW, Jin ES, Chen P-H, Sullivan LB, Cheng T, et al. Reductive carboxylation supports growth in tumour cells with defective mitochondria. Nature. 2011 Nov;481:385–9.

14. Wise DR, Ward PS, Shay JES, Cross JR, Gruber JJ, Sachdeva UM, et al. Hypoxia promotes isocitrate dehydrogenase-dependent carboxylation of -ketoglutarate to citrate to support cell growth and viability. Proc Natl Acad Sci. 2011 Dec;108(49):19611–6.

15. Metallo CM, Gameiro PA, Bell EL, Mattaini KR, Yang J, Hiller K, et al. Reductive glutamine metabolism by IDH1 mediates lipogenesis under hypoxia. Nature. 2011 Nov;481:380–6.

16. Fendt S-M, Bell EL, Keibler MA, Olenchock BA, Mayers JR, Wasylenko TM, et al. Reductive glutamine metabolism is a function of the α-ketoglutarate to citrate ratio in cells. Nat Commun. 2013 Jul;4. Available from: http://www.nature.com/doifinder/10.1038/ncomms3236

17. Mullen AR, Hu Z, Shi X, Jiang L, Boroughs LK, Kovacs Z, et al. Oxidation of Alpha-Ketoglutarate Is Required for Reductive Carboxylation in Cancer Cells with Mitochondrial Defects. Cell Rep. 2014 Jun;7(5):1679–90.

18. Hellwig-Bürgel T, Rutkowski K, Metzen E, Fandrey J, Jelkmann W. Interleukin-1β and Tumor Necrosis Factor-a Stimulate DNA Binding of Hypoxia-Inducible Factor-1. Blood. 1999;94(5):1561–7.

19. Jung Y, Isaacs JS, Lee S, Trepel J, Liu Z, Neckers L. Hypoxia-inducible factor induction by tumour necrosis factor in normoxic cells requires receptor-interacting protein-dependent nuclear factor κB activation. Biochem J. 2003 Mar;370(3):1011.

20. Simon MC. Diverse Effects of Hypoxia on Tumor Progression. Berlin, Heidelberg: Springer Berlin Heidelberg; 2010. Available from: http://link.springer.com/10.1007/978-3-642-13329-9

21. Nishi K, Oda T, Takabuchi S, Oda S, Fukuda K, Adachi T, et al. LPS Induces Hypoxia-Inducible Factor 1 Activation in Macrophage-Differentiated Cells in a Reactive Oxygen Species–Dependent Manner. Antioxid Redox Signal. 2008 Jan;10(5):983–96.

22. Walther JL, Metallo CM, Zhang J, Stephanopoulos G. Optimization of 13C isotopic tracers for metabolic flux analysis in mammalian cells. Metab Eng. 2012 Mar;14(2):162–71.

23. Metallo CM, Walther JL, Stephanopoulos G. Evaluation of 13C isotopic tracers for metabolic flux analysis in mammalian cells. J Biotechnol. 2009 Nov;144(3):167–74.

24. Sapcariu SC, Kanashova T, Weindl D, Ghelfi J, Dittmar G, Hiller K. Simultaneous extraction of proteins and metabolites from cells in culture. MethodsX. 2014;1:74–80.

25. Hiller K, Hangebrauk J, Jäger C, Spura J, Schreiber K, Schomburg D. MetaboliteDetector: comprehensive analysis tool for targeted and nontargeted GC/MS based metabolome analysis. Anal Chem. 2009;81(9):3429–39.

26. Leek RD, Harris AL. Tumor-Associated Macrophages in Breast Cancer. J Mammary Gland Biol Neoplasia. 2002 Apr;7(2):177–89.

27. Lewis JS, Lee JA, Underwood JC, Harris AL, Lewis CE. Macrophage responses to hypoxia: relevance to disease mechanisms. J Leukoc Biol. 1999;66(6):889–900.

28. Murdoch C. Mechanisms regulating the recruitment of macrophages into hypoxic areas of tumors and other ischemic tissues. Blood. 2004 Jun;104(8):2224–34.

29. Palsson-McDermott EM, Curtis AM, Goel G, Lauterbach MAR, Sheedy FJ, Gleeson LE, et al. Pyruvate Kinase M2 Regulates Hif-1α Activity and IL-1β Induction and Is a Critical Determinant of the Warburg Effect in LPS-Activated Macrophages. Cell Metab. 2015 Jan;21(1):65–80.

30. Strelko CL, Lu W, Dufort FJ, Seyfried TN, Chiles TC, Rabinowitz JD, et al. Itaconic acid is a mammalian metabolite induced during macrophage activation. J Am Chem Soc. 2011;133(41):16386–9.

31. Blouin CC. Hypoxic gene activation by lipopolysaccharide in macrophages: implication of hypoxia-inducible factor 1. Blood. 2003 Oct;103(3):1124–30.

32. Kim J, Tchernyshyov I, Semenza GL, Dang CV. HIF-1-mediated expression of pyruvate dehydrogenase kinase: A metabolic switch required for cellular adaptation to hypoxia. Cell Metab. 2006 Mar;3(3):177–85.

33. Patel MS, Korotchkina LG. Regulation of the pyruvate dehydrogenase complex. Biochem Soc Trans. 2006 Apr;34(Pt 2):217–22.

34. King A, Selak MA, Gottlieb E. Succinate dehydrogenase and fumarate hydratase: linking mitochondrial

dysfunction and cancer. Oncogene. 2006;25(34):4675–82.

35. Demaria M, Giorgi C, Lebiedzinska M, Esposito G, D'Angeli L, Bartoli A, et al. A STAT3-mediated metabolic switch is involved in tumour transformation and STAT3 addiction. Aging. 2010 Nov;2(11):823–42.

36. Garzetti L, Menon R, Finardi A, Bergami A, Sica A, Martino G, et al. Activated macrophages release microvesicles containing polarized M1 or M2 mRNAs. J Leukoc Biol. 2014 May;95(5):817–25.

37. O'Neill LAJ, Hardie DG. Metabolism of inflammation limited by AMPK and pseudo-starvation. Nature. 2013 Jan;493(7432):346–55.

38. Yang C, Ko B, Hensley CT, Jiang L, Wasti AT, Kim J, et al. Glutamine Oxidation Maintains the TCA Cycle and Cell Survival during Impaired Mitochondrial Pyruvate Transport. Mol Cell. 2014 Nov;56(3):414–24.

39. Vats D, Mukundan L, Odegaard JI, Zhang L, Smith KL, Morel CR, et al. Oxidative metabolism and PGC-1β attenuate macrophage-mediated inflammation. Cell Metab. 2006 Jul;4(1):13–24.

40. Tan Z, Xie N, Cui H, Moellering DR, Abraham E, Thannickal VJ, et al. Pyruvate dehydrogenase kinase 1 participates in macrophage polarization via regulating glucose metabolism. J Immunol Baltim Md 1950. 2015 Jun 15;194(12):6082–9.

41. Everts B, Amiel E, Huang SC-C, Smith AM, Chang C-H, Lam WY, et al. TLR-driven early glycolytic reprogramming via the kinases TBK1-IKKε supports the anabolic demands of dendritic cell activation. Nat Immunol. 2014 Feb;15(4):323–32.

42. Infantino V, Paolo C, Liana C, Maria AP, Maria ADN, Rosa C, et al. The mitochondrial citrate carrier: a new player in inflammation. Biochem J. 2011;438(3):433–6.

43. Wise DR, Thompson CB. Glutamine Addiction: A New Therapeutic Target in Cancer. Trends Biochem Sci. 2010 Aug;35(8):427–33.

44. Newsholme P, Curi R, Pithon Curi TC, Murphy CJ, Garcia C, Pires de Melo M. Glutamine metabolism by lymphocytes, macrophages, and neutrophils: its importance in health and disease. J Nutr Biochem. 1999 Jun;10(6):316–24.

45. Jha AK, Huang SC-C, Sergushichev A, Lampropoulou V, Ivanova Y, Loginicheva E, et al. Network Integration of Parallel Metabolic and Transcriptional Data Reveals Metabolic Modules that Regulate Macrophage Polarization. Immunity. 2015 Mar;42(3):419–30.

46. Krawczyk CM, Holowka T, Sun J, Blagih J, Amiel E, DeBerardinis RJ, et al. Toll-like receptor–induced changes in glycolytic metabolism regulate dendritic cell activation. Blood. 2010 Jun;115(23):4742–9.

47. Gameiro PA, Laviolette LA, Kelleher JK, Iliopoulos O, Stephanopoulos G. Cofactor balance by nicotinamide nucleotide transhydrogenase (NNT) coordinates reductive carboxylation and glucose catabolism in the tricarboxylic acid (TCA) cycle. J Biol Chem. 2013;288(18):12967–77.

48. West AP, Brodsky IE, Rahner C, Woo DK, Erdjument-Bromage H, Tempst P, et al. TLR signalling augments macrophage bactericidal activity through mitochondrial ROS. Nature. 2011 Apr;472(7344):476–80.

49. Houtkooper RH, Cantó C, Wanders RJ, Auwerx J. The Secret Life of NAD+: An Old Metabolite Controlling New Metabolic Signaling Pathways. Endocr Rev. 2010 Apr;31(2):194–223.

50. Clementi E, Brown GC, Feelisch M, Moncada S. Persistent inhibition of cell respiration by nitric oxide: crucial

role of S-nitrosylation of mitochondrial complex I and protective action of glutathione. Proc Natl Acad Sci. 1998;95(13):7631–6.

51. Drapier JC, Hibbs JB. Differentiation of murine macrophages to express nonspecific cytotoxicity for tumor cells results in L-arginine-dependent inhibition of mitochondrial iron-sulfur enzymes in the macrophage effector cells. J Immunol. 1988 Apr;140(8):2829–38.

FIGURE 1. **Metabolome analysis of RAW264 macrophages in the context of LPS activation and hypoxia.** Analysis of intracellular metabolite abundance in RAW264 cells, cultivated under normoxia (21% O_2) and hypoxia (2% O_2), unstimulated or stimulated with LPS. Metabolites were extracted and analyzed by GC/MS. Signal intensities (peak area) are normalized to unstimulated cells under normoxia. Cells were treated with 10 ng/ml LPS for 6 hours. Error bars indicate SEM (Welsh's t-Test, * $p < 0.01$, $n = 3$ wells). One representative experiment with three individual wells per condition is presented. The experiment was performed three times.

FIGURE 2. **Expression analysis of pro-inflammatory associated genes.** (A) Relative gene expression of *Irg1*. (B) Western blot against Irg1/Cad, the protein that catalyzes the conversion of *cis*-aconitate to itaconate (no significant difference (data not shown)). (C-F) Relative gene expression of *Tnfα, iNos, Il1ß* and *Hif1α,* normalized to normoxia Ctrl (-LPS). Error bars indicate SEM (Welsh's *t*-Test, * $p < 0.01$, $n = 3$). Gene expression data represents the mean over three independent experiments.

FIGURE 3. **Pdh flux analysis in M(LPS) macrophages.** (A) Schematic of atom transitions in central metabolism using [U-^{13}C]glucose as a tracer for determination of mass isotopomer distributions (MIDs) to infer relative intracellular fluxes. ^{13}C carbons are in grey, ^{12}C in black. The dotted line indicates end of one route. Aco: aconitase; Idh: isocitrate dehydrogenase; Akgdh: aKG dehydrogenase; OA: oxaloacetate. (B) MID of citrate. M0 – M6 indicates the different mass isotopologues. (C) gene expression analysis of *Pdk1*. (D-H) Western Blot analysis of Pdk1 and Pdh phosphorylation on Ser232, 293 and 300. α-Tubulin serves as loading control. (D) shows one representative western Blot of three independent experiments. (E-H) shows quantification of three independent experiments. (I) Ratio of M2 citrate/M3 pyruvate indicating relative pyruvate oxidation through Pdh. (J-K) MID of aKG and Malate. (L) Absolute quantification of glucose uptake and lactate release, and ratio of lactate release/glucose uptake to infer fractional lactate formation per glucose. (M) Activation of RAW264 cells with 10 ng/ml LPS or 50 ng/ml interferon-γ (Inf) in medium with [U-^{13}C]glucose. Presented are citrate M2 isotopologues as a readout for relative glucose flux through Pdh. (N) Relative gene expression of *Pdk1* normalized to normoxia Ctrl (-LPS). Error bars indicate SEM. (Welsh's t-Test, * $p < 0.01$, $n = 3$). One representative experiment with three individual wells per condition is presented. Each experiment was performed at least three times, except for (C): Presented is the mean +/-SEM over three independent experiments. (Welsh's *t*-Test, * $p < 0.01$, $n = 3$)

FIGURE 4. **Contribution of glutamine to central metabolism in M(LPS) macrophages.** (A) Schematic of atom transitions in central metabolism using [U-^{13}C]glutamine as a tracer. ^{13}C carbons are in grey, ^{12}C in black. Citrate molecules derived from reductive carboxylation of aKG are M5 isotopologues, whereas citrate molecules from the oxidative route of the TCA cycle are M4 isotopologues. The dotted line indicates end of one route. Aco: aconitase; Idh: isocitrate dehydrogenase; Akgdh: aKG dehydrogenase; Acly: ATP dependent citrate lyase; FA: Fatty acid. (B) MID of citrate. M0 – M6 indicates the different mass isotopologues. (C-D) Determination of oxidative TCA cycle activity: ratio of M4 citrate/M5 glutamate and Ratio of M5 citrate/M5 glutamate indicating relative reductive Idh flux. (E-F) MID of malate and aKG (G-I) Absolute quantification of glutamine uptake, glutamate release and uptake of the branched chain amino acids (valine, isoleucine and leucine). (J) Carbon contribution (%) of glucose, glutamine and other carbon sources to citrate, aKG, malate and itaconate. Carbon contributions are based on MIDs from [U-^{13}C]glucose labeling (Figure 3) and [U-^{13}C]glutamine labeling. Carbon contribution to itaconate under non-LPS conditions should not be considered since itaconate levels are negligible low under these non-stimulated conditions (Figure 1A). Error bars indicate SEM (Welsh's t-Test, * $p < 0.01$, $n = 3$). One representative experiment with three individual wells per condition is presented. Each experiment was performed at least three times.

FIGURE 5. **Morphological changes upon LPS activation require sustained lipogenesis in macrophages.** (A) Microscopy (brightfield image) of RAW macrophages unstimulated or stimulated with 10 ng/ml LPS for 6h. White bar indicates 100 µm (B) Mean average of cell size [pixels] (left) and analysis of adhesion index (right) of LPS stimulated and non-stimulated cells, obtained from brightfield microscopy. Analysis demonstrates morphological adaption of macrophages during LPS activation. For further details regarding the analysis approach see experimental procedures. (C) Relative gene expression of *carnitine palmitoyl transferase1* (*Cpt1*) normalized to normoxia Ctrl (-LPS), indicating inhibition of ß-oxidation upon LPS stimulation. (D-E) MID of palmitate using (D) [U-^{13}C]glucose and (E) [U-^{13}C]glutamine as a tracer. Contribution of each carbon source is depicted in the top right corner of each panel. Error bars indicate SEM (Welsh's t-Test, * $p < 0.01$, $n \geq 3$). One representative experiment with three individual wells per condition is presented. Each experiment was performed at least three times; except for (C): Presented is the mean +/-SEM over three independent experiments. (Welsh's *t*-Test, * $p < 0.01$, $n = 3$).

FIGURE 6. **Inhibition of pyruvate transport into mitochondria suppresses pro-inflammatory responses in M(LPS) macrophages.** (A) Application of the specific pyruvate transport inhibitor UK5099 to inhibit flux through Pdh. Cells were treated with 100 µM UK5099 for 6h with or without 10 ng/ml LPS at normoxia. Prior to treatment start, cells were cultivated for 24h in [U-^{13}C]glucose. Presented are citrate M2 isotopologues as a readout for relative glucose flux through Pdh. (B-D) Intracellular metabolite levels of citrate, itaconate and succinate upon LPS stimulation and after application of 100 µM UK5099. Metabolite levels were determined using GC/MS and normalized to cell number. (E-J) Relative gene expression of *Il1ß, iNos, Irg1, Tnfα, Cpt1* and *Pdk1* normalized to normoxia Ctrl (-LPS), upon LPS stimulation and after application of 100 µM UK5099 for 6h. (K) Viability assay to test a potential effect of UK5099 on cell viability. Assay was performed using Trypan blue, dead and live cells were counted. (L) To validate the effect of UK5099 a modified experimental setup has additionally been performed. Cells were first activated with 10ng/ml LPS for 3h and then UK5099 was added to the cells for additional 6h. In total, LPS activation was 9h in this case. Non-UK5099 treated and non-activated cells served as control. (M-O) Intracellular metabolite levels for citrate, itaconate and succinate (analysis as in (B-D)). (P-S) Relative gene expression analysis of *Tnfα , iNos, Irg1* and *Il1ß*. (T-U) MID of Palmitate using [U-^{13}C]glucose as a tracer. Experimental setup as in (A). (U) Glucose contribution to palmitate, determined from (T). Error bars indicate SEM (Welsh's *t*-Test, * $p < 0.01$, $n = 3$). One representative experiment with three individual wells per condition is presented. Each experiment was performed at least three times.

FIGURE 7**. Model summarizing the metabolic adaptations in M(LPS) macrophages**. Resting cells use glucose via Pdh and TCA oxidation for energy production. Depending on the cell type, anabolic processes run in parallel. Hypoxic cells and cancer cells with stabilized Hif1α, increase their glycolytic rate, inhibit Pdh flux and use glutamine derived carbon for increased reductive carboxylation of aKG for subsequent lipogenesis. Highly proliferating cells promote anabolic processes to support proliferation. M(LPS) macrophages show stabilized Hif1α but do not decrease pyruvate oxidation through Pdh. Under this condition Hif1α does not increase PDk1 abundance. Compared to resting cells, less citrate is oxidized through the TCA cycle and is rerouted to serve as a precursor for itaconate and fatty acid synthesis. Glutamine serves to replenish the TCA cycle by increasing its carbon contribution to aKG and subsequent metabolites. BCAAs might also support carbon supply to the TCA cycle but this needs additional research. Despite sustained pyruvate oxidation through Pdh, oxygen consumption rates are lower than in resting cells.

TABLE1. **Primer sequences used for qPCR**

Gene	5' – 3' sequence
L27_F	ACATTGACGATGGCACCTC
L27_R	GCTTGGCGATCTTCTTCTTG
IRG1_F	GCAACATGATGCTCAAGTCTG
IRG1_R	TGCTCCTCCGAATGATACCA
TNFa_F	GGTTCTGTCCCTTTCACTCAC
TNFa_R	TGCCTCTTCTGCCAGTTCC
iNOS_F	AGCCCTCACCTACTTCCTG
iNOS_R	CAATCTCTGCCTATCCGTCTC
PDK1_F	TGCAAAGTTGGTATATCCAAAGCC
PDK1_R	ACCCCGAAGCTCTCCTTGTA
IL1b_F	TGCCACCTTTTGACAGTGATG
IL1b_R	TGATGTGCTGCTGCGAGATT
CPT1_F	TGGCAGTCGACTCACCTTTC
CPT1_R	CAAACAGTTCCACCTGCTGC
HIF1a_F	TGACGGCGACATGGTTTACA
HIF1a_R	AATATGGCCCGTGCAGTGAA

FIGURE 1

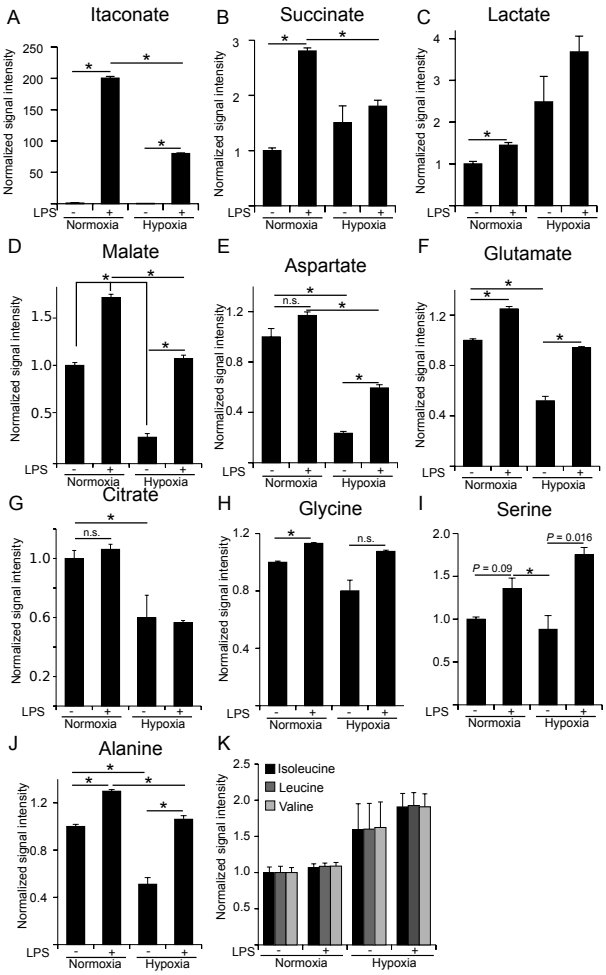

FIGURE 2

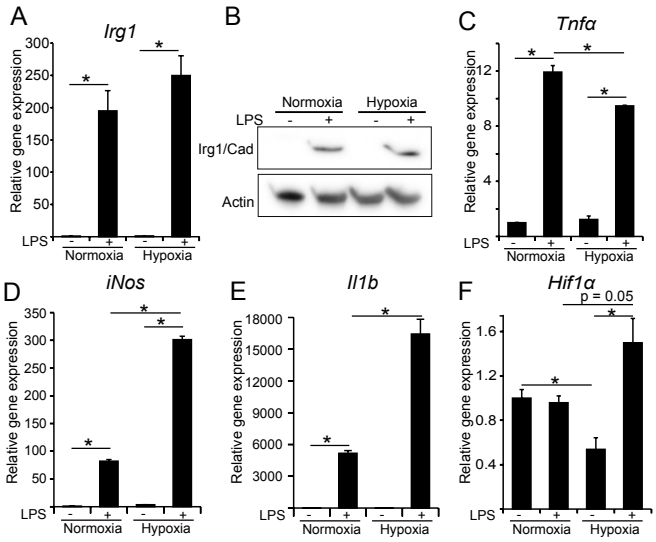

FIGURE 3

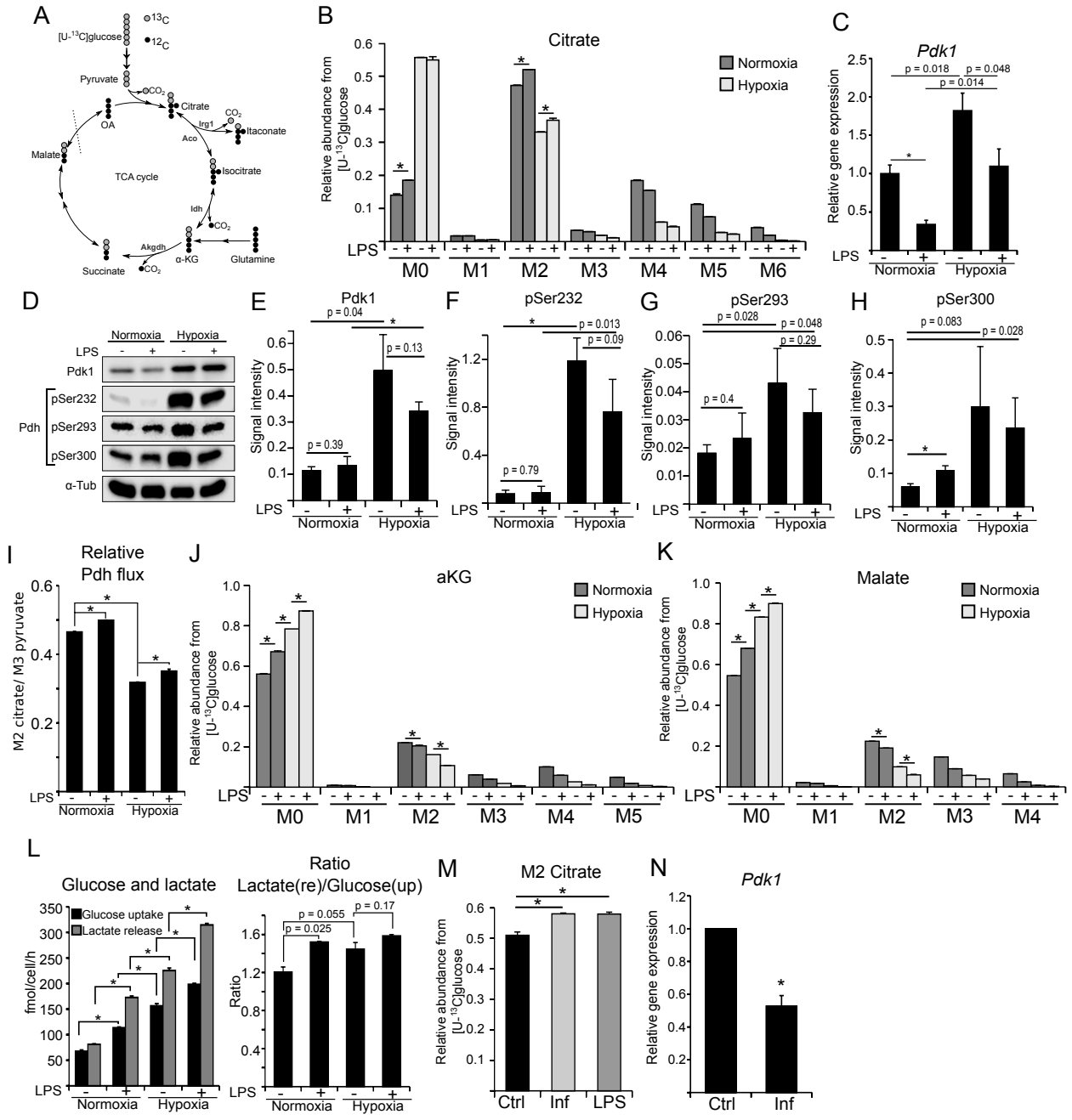

FIGURE 4

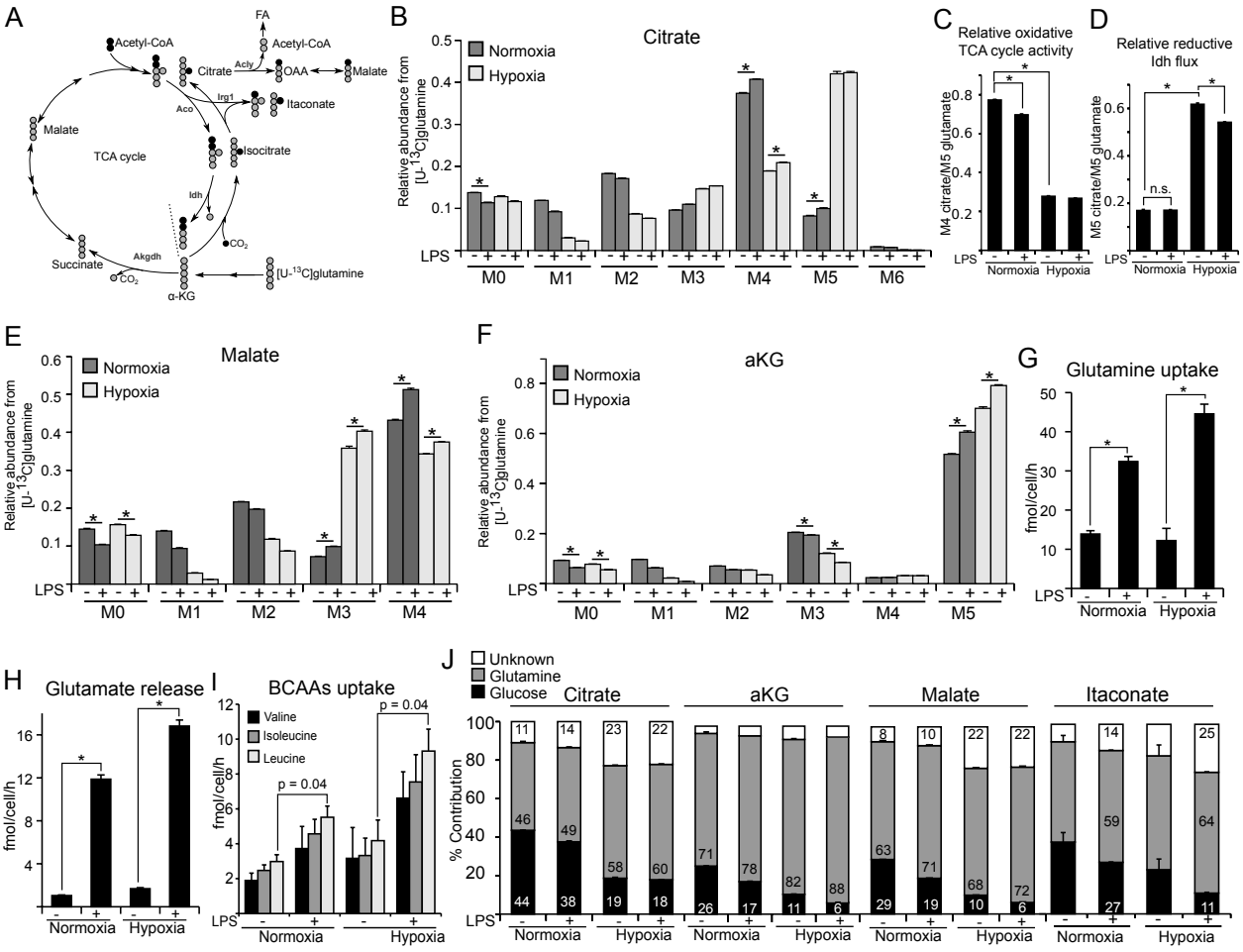

FIGURE 5

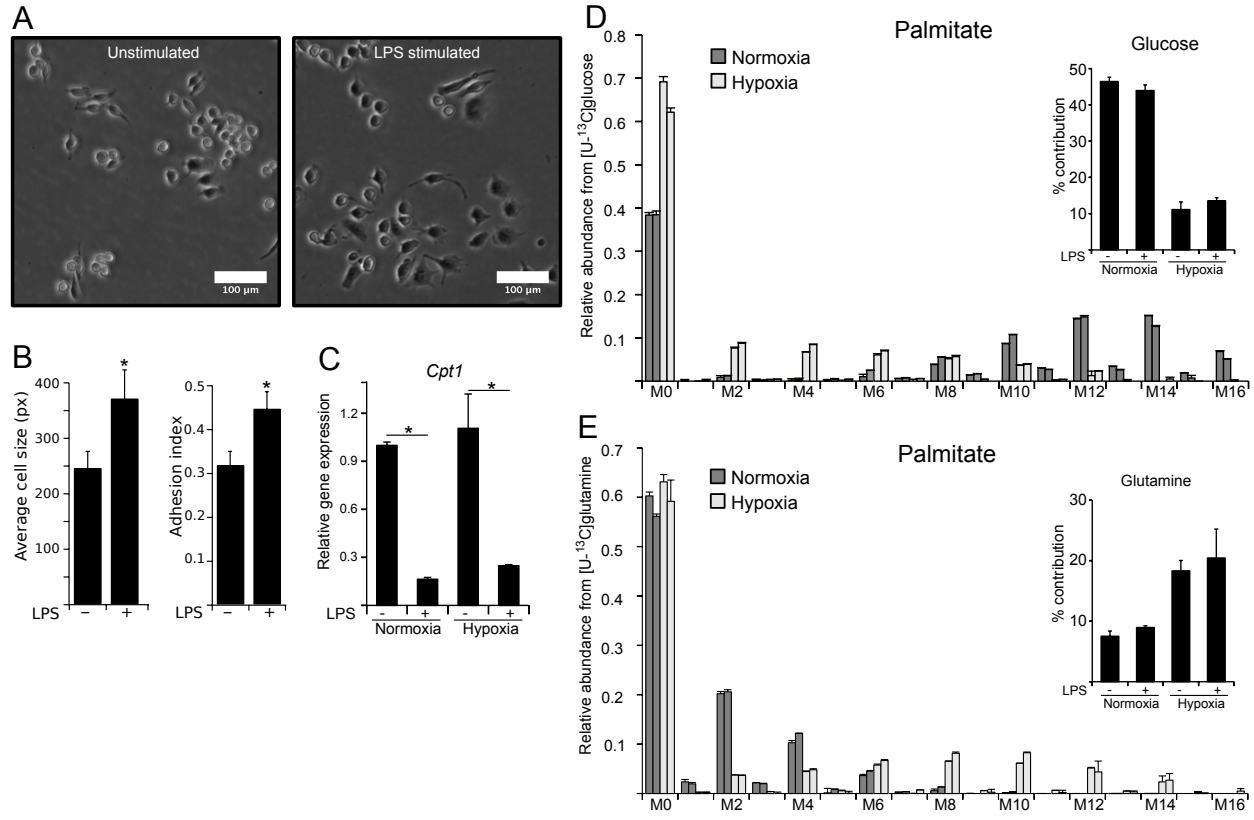

FIGURE6

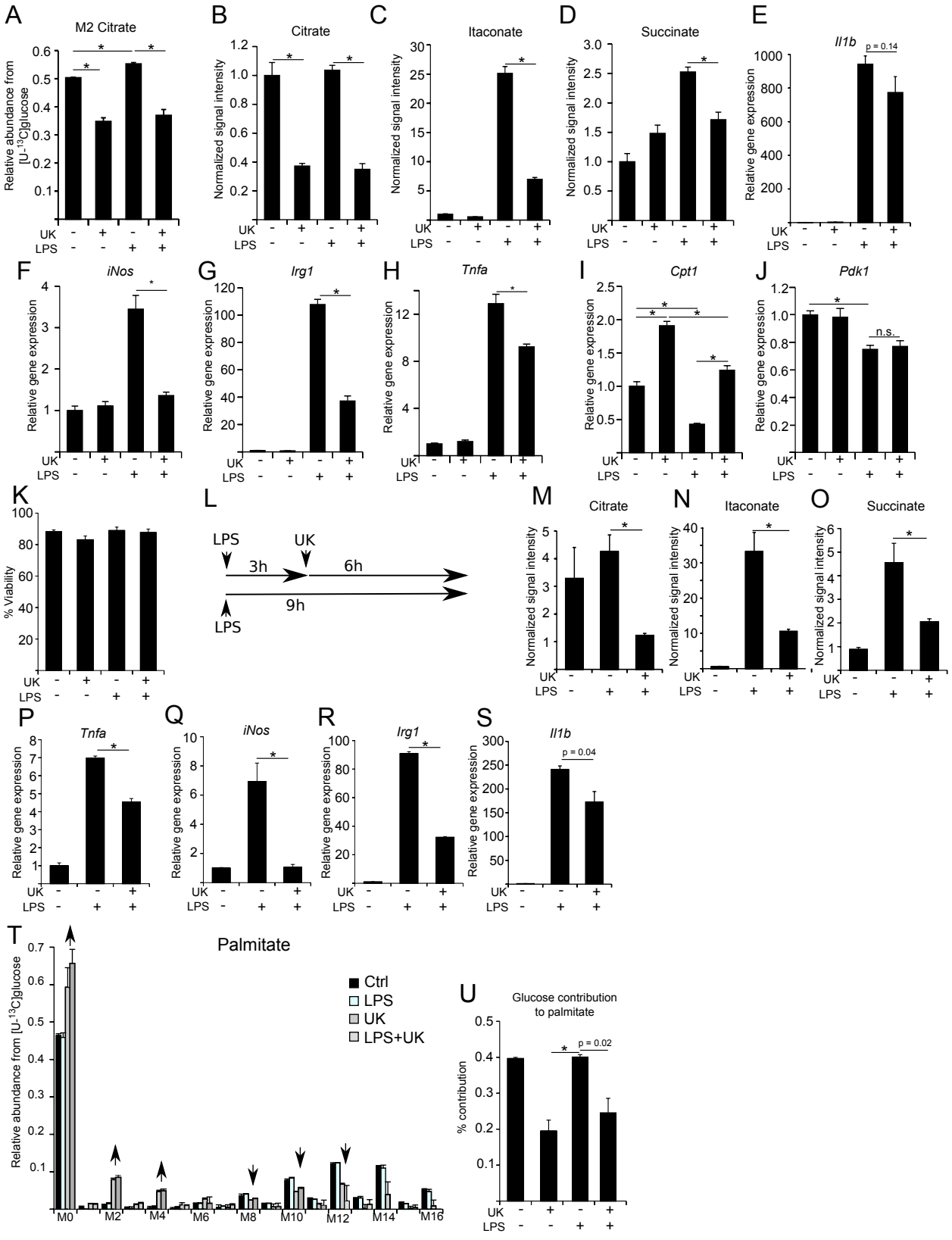

FIGURE7

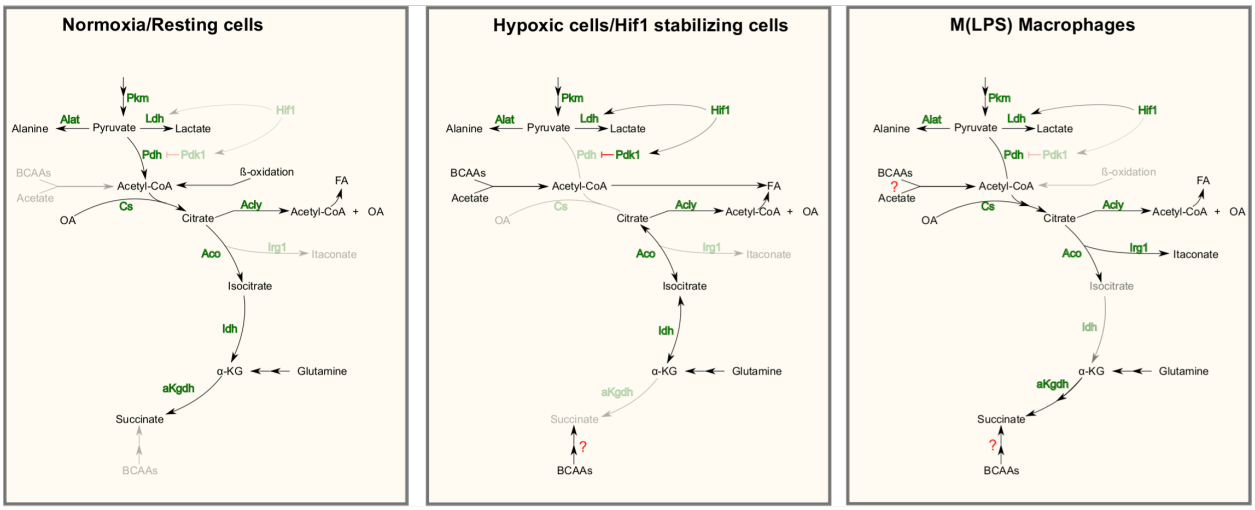

Metabolism:

Pro-inflammatory macrophages sustain pyruvate oxidation through pyruvate dehydrogenase for the synthesis of itaconate and to enable cytokine expression

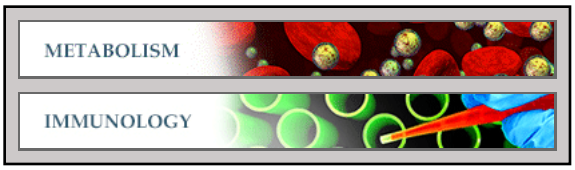

Johannes Meiser, Lisa Krämer, Sean C. Sapcariu, Nadia Battello, Jenny Ghelfi, Aymeric Fouquier D'Herouel, Alexander Skupin and Karsten Hiller

J. Biol. Chem. published online December 17, 2015

Access the most updated version of this article at doi: 10.1074/jbc.M115.676817